CDF note 10235

A Search for the Standard Model Higgs Boson in the Process $ZH \to \ell^+\ell^- b\bar{b}$ Using 5.7 fb^{-1} of CDF II Data

The CDF Collaboration
URL http://www-cdf.fnal.gov
(Dated: July 16, 2010)

We present a search for the standard model (SM) Higgs boson in the associated production process $p\bar{p} \to ZH \to \ell^+\ell^- b\bar{b}$ using 5.7 fb^{-1} of Tevatron data collected with the CDF II detector. We select events containing Z candidates reconstructed from e^+e^- or $\mu^+\mu^-$ pairs and containing at least two energetic jets. We form our final analysis sample by requiring events to contain at least one b-tagged jet. To enhance the discriminating power of the jet energies and associated quantities, we apply a neural network (NN) derived correction to the jets which depends on the missing transverse energy and its orientation with respect to the jets. We employ two dimensional NNs to simultaneously separate signal events from the dominant $Z+jets$ and kinematically different $t\bar{t}$ backgrounds. These NNs use various kinematic distributions, matrix element probabilities and the output of a separate jet flavor separating NN as inputs. We find good agreement between the observed data and the predicted SM backgrounds and set 95% confidence level upper limits on the Higgs production cross section (σ_{ZH}) times the branching ratio for $H \to b\bar{b}$. For a Higgs boson mass of 115 Gev/c^2, we observe (expect) a 95% confidence level upper limit of 6.55 $\times$ SM (5.98 $\times$ SM).

Preliminary Results for Summer 2010 Conferences

I. INTRODUCTION

The evidence for the mechanism of spontaneous symmetry breaking has yet to be resolved in the standard model of particle physics (SM). The simplest theory provides for a Higgs boson to meet these requirements [1], [2], and [3]. For masses $\lesssim$ 135 GeV/c^2, the Higgs boson decays largely to $b\bar{b}$ at the Tevatron [4]. However, these b-quarks alone are obscured by large QCD backgrounds. In an attempt to distinguish Higgs events, Higgs boson produced along with a Z or W boson are often searched for even though the cross-section is several times lower. In this note, we present the results of an updated search for the SM Higgs in the process $ZH \rightarrow \ell^+\ell^- b\bar{b}$. This process has the added benefit of all of the decay products being measurable with the invariant mass of the leptons having a Z mass resonance and the dijet invariant mass producing a Higgs boson mass resonance. This analysis updates the previous search with 4.1 fb^{-1} [5]. The following sections detail the event selection, data model, application of multivariate techniques, uncertainties, and results.

II. DATA SAMPLE & EVENT SELECTION

In this analysis, we use data collected at CDF (Collider Detector at Fermilab) from February 4, 2002 to February 25, 2010 corresponding to 5.7 fb^{-1}. Given that we require leptons in the final state, we use data saved due to their high-P_T [7] lepton characteristics. This triggered data require at least one central ($|\eta| < 1.1$) muon candidate with $P_T \geq 18$ GeV/c, one central electron candidate with $E_T \geq 18$ GeV, or two calorimeter deposits [8] ≥ 18 GeV within $|\eta| \leq 3.6$ in order to be saved. Since the leptons in our signature come from a Z boson decay, we look for two same-flavor leptons reconstructing to roughly the Z mass ($76 \leq M_{\ell\ell} \leq 106$ GeV/c^2). For events where both leptons are central, we further require opposite charges due to better curvature measurement. Since taus decay within the detector, we only explicitly search for electrons and muons. Due to varying quality of the lepton selection, two categories are created to improve final limits. The high $S/\sqrt{B}$ lepton category largely includes dimuon and events with a tight central electron. The low $S/\sqrt{B}$ category includes Z's made from plug and loose central electrons or events with a tight central electron and a track-based electron pointing toward an uninstrumented region of the detector. The jet selection is summarized in Table I.

Jet Selection for Pre-Tag Region
2 or more Cone 0.4 jets with $E_T > 15$ GeV, $\|\eta\| > 2$
1 of these jets with $E_T > 25$ GeV

TABLE I. Summary of jet selection.

This signature also requires that there be at least two jets. Our selection looks for jets within $|\eta| \leq 2.0$. One jet must have E_T (dR cone 0.4) ≥ 25 GeV, whereas a second must have $E_T \geq 15$ GeV. Events meeting this selection of two leptons and two jets make up our "Pre-tag" category. While it contains events in our final analysis channels, the statistics are so much higher that it serves as a model validation.

To reduce background in our final analysis channels, we look for the jets to have characteristics of originating from a b-quark. Within the detector, b-quarks hadronize before decaying producing a displaced vertex. Detection of a b-quark is referred to as b-tagging. We use two b-tagging algorithms: SecVtx (secondary vertex) [9], and JetProb (the probability the jet originated from the primary vertex) [10]. In an effort to increase acceptance, we check for three b-tagging categories. First, we see if an event has two tight SecVtx tags (TT). If not, then we check for one loose SecVtx tag and one JetProb tag $\leq 5\%$ (L+JP). If both fail, we check for one tight SecVtx tag (T) in order to enter the final selection. These three b-tag categories combined with the two lepton selection categories lead to six final analysis channels (see Table II).

Signal Region	Z Quality	b-tag Requirements
TT High	High S/B	2 Tight SecVtx Tags
L+JP High	High S/B	1 Loose SecVtx Tag + 1 JetProbability Tag
T High	High S/B	1 Tight SecVtx Tag
TT Low	Low S/B	2 Tight SecVtx Tags
L+JP Low	Low S/B	1 Loose SecVtx Tag + 1 JetProbability Tag
T Low	Low S/B	1 Tight SecVtx Tag

TABLE II. The six final analysis channels used in this analysis.

III. DATA MODEL

Background processes possessing a detector signature similar to the signal are mainly those which contain two leptons and two (or more) jets in the final state. The dominant background is $Z + jets$, with Z + lights flavor jets (u, d, s) forming the major background component before b-tag requirements are imposed. $Z + jets$ events are modeled using an ALPGEN v2.10 prime MC [11] with PYTHIA [12] 6.325 for showering. Signal, diboson (ZZ, WZ, WW), and $t\bar{t}$ processes are modeled with PYTHIA 6.216 MC. The $t\bar{t}$ simulation assumes a top mass of 175 GeV/c^2.

The probability of a jet to "fake" an electron is measured in independent jet-triggered data samples (as a function of jet E_T) and applied to the jets in our selected events forming the "fake" $Z \to ee$ contribution. The fake $Z \to \mu\mu$ contribution is formed from events with like-sign muon pairs. The agreement between our model and observed data is checked across a variety of kinematic distributions, some of which are shown in Figures 2 and 1. Table III lists the predicted number of events from major backgrounds and the number of observed events at pre-tag.

	High $S/\sqrt{B}$	Low $S/\sqrt{B}$
ZH	5.8 ± 0.6	1.0 ± 0.1
$t\bar{t}$	75.9 ± 9.6	41.4 ± 5.2
WW	6.5 ± 0.6	5.7 ± 0.6
WZ	151.8 ± 14.9	35.1 ± 3.4
ZZ	154.3 ± 15.1	31.1 ± 3.1
$Z \to \ell\ell + b\bar{b}$	508.1 ± 207.0	104.5 ± 42.6
$Z \to \ell\ell + c\bar{c}$	935.7 ± 381.3	198.4 ± 80.8
$Z \to \ell\ell + l.f.$	13686.7 ± 2737.3	3050.5 ± 610.1
fakes	707.3 ± 353.7	691.7 ± 345.9
Total Bkg	16226.5 ± 2794.1	4158.3 ± 707.3
Total Data	16802	4300

TABLE III. Model and data acceptance before b-tagging is imposed.

After b-tag selection, the contribution from Z + light flavor jets (mistagged jets) is modeled using re-weighted pre-tag data events, with the weights reflecting the probability for a light flavor jet to be tagged as a b-jet. These probabilities are measured for each b-tag algorithm in independent jet triggered data samples.

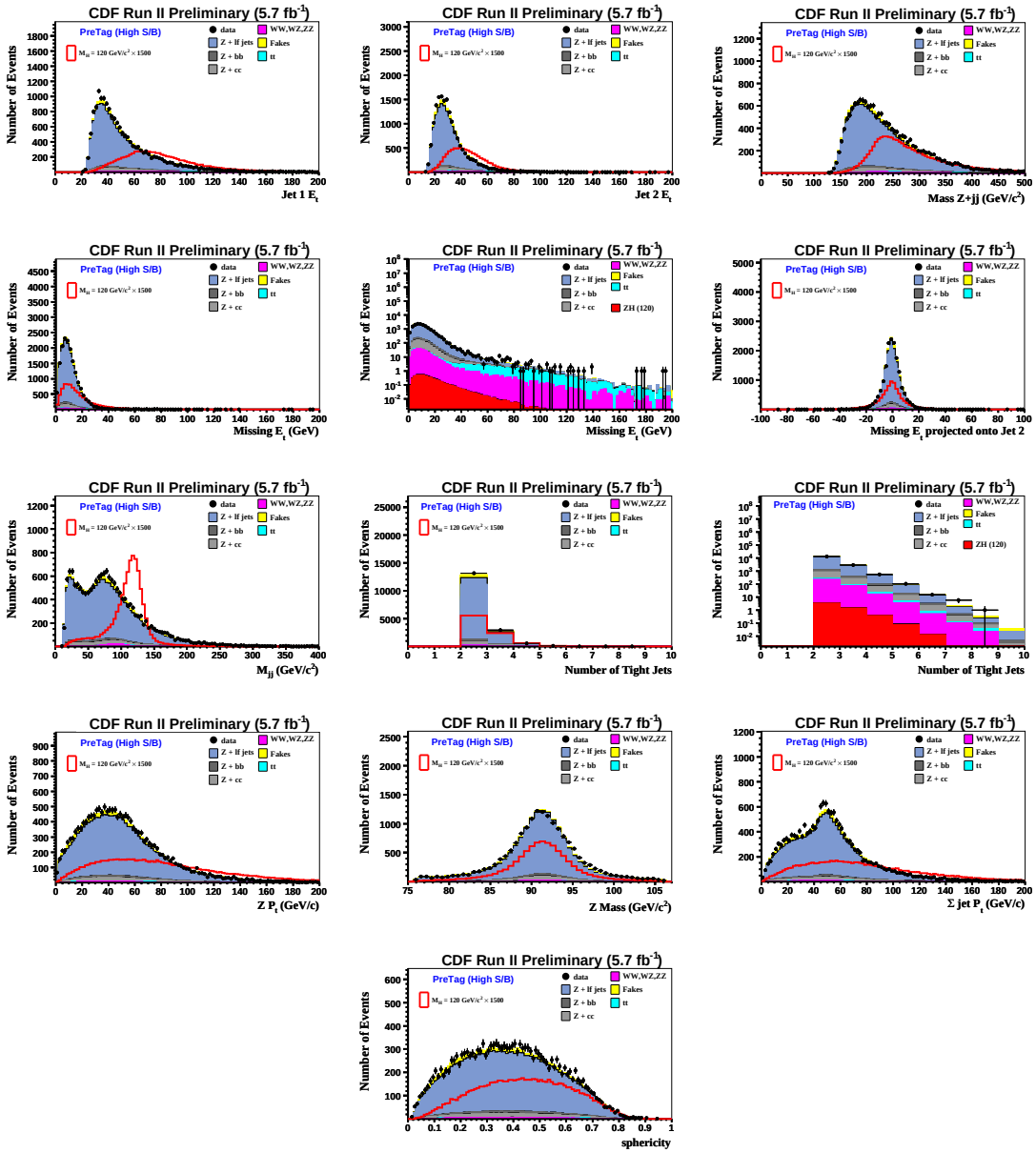

FIG. 1. Selected distributions showing the agreement between the data and model for the pre-tag High S/B selection.

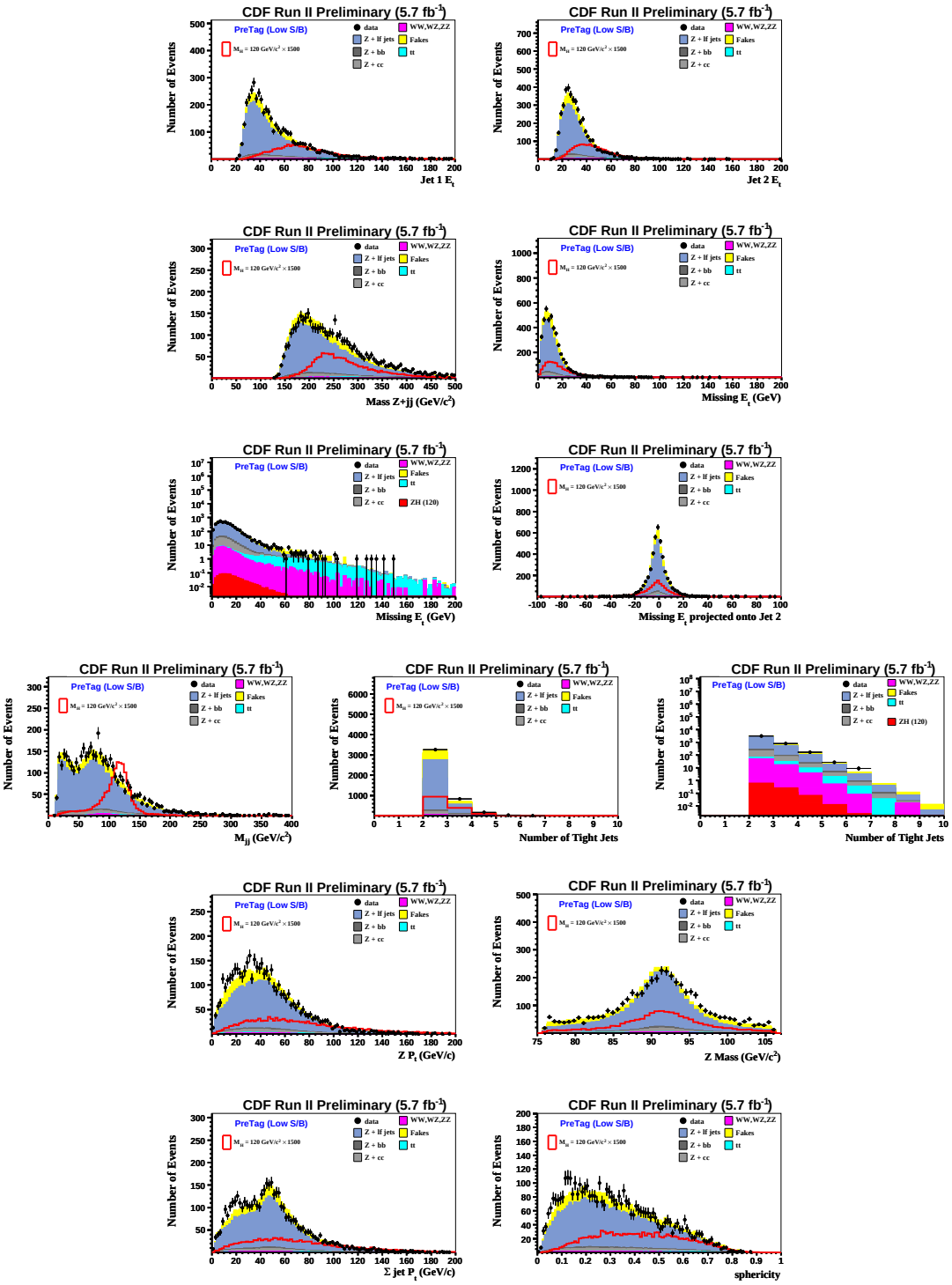

FIG. 2. Selected distributions showing the agreement between the data and model for the pre-tag Low S/B selection.

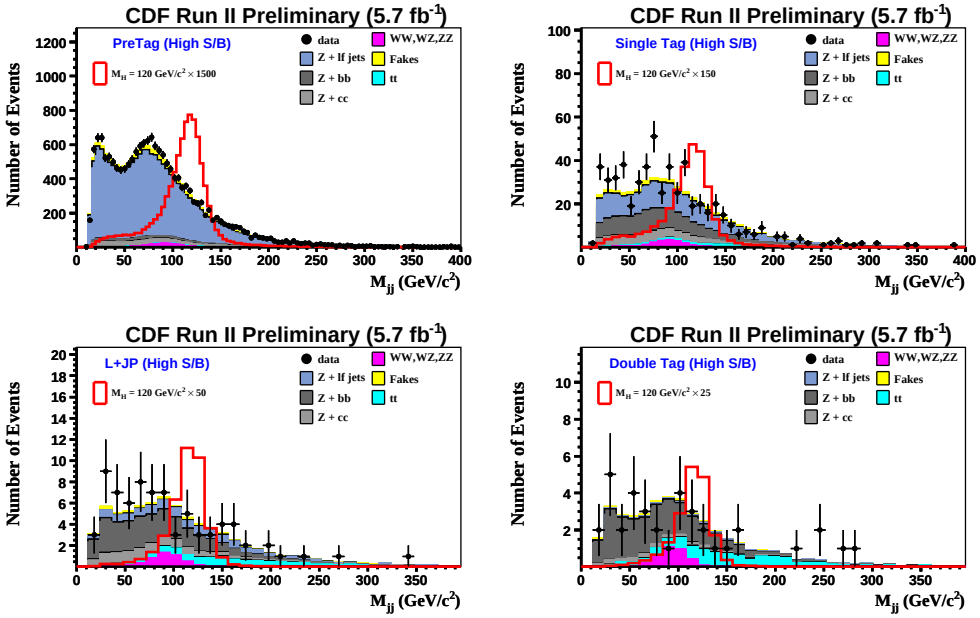

FIG. 3. Effect of NN jet energy corrections on the dijet mass distributions.

IV. MULTIVARIATE TECHNIQUES

A. Jet Energy Corrections

The dijet mass (M_{jj}) is one of the most useful distributions for ZH vs. $Z + jets$ discrimination, with its separating power limited mainly by the jet-energy resolution. In general, incorrect measurement of jet energies can result in over-estimation of the missing transverse energy ($\not\!\!E_T$). In order to improve the dijet mass resolution, we correct the energies of the leading and second E_T jets by factors which depend upon the direction and magnitude of the $\not\!\!E_T$, as well as its transverse projection onto the jets. The correction factors are the output values of an MLPfit [13] Neural Network derived function. All kinematic quantities (except for $\not\!\!E_T$) are computed using the NN corrected jet energies. The effect of these corrections on the dijet mass can be seen in Figure 3.

B. Flavor Separator NN

In previous iterations of this analysis, the single tag categories have suffered from low S/B due to the presence of large ($\sim 40\%$) backgrounds from incorrectly tagged light flavor jet events. In order to increase the ability of our final analysis discriminants (2D-NN discussed in section IV D) to separate background from signal, we include (as a potential) 2D-NN input, the output of the Karlsruhe Neural Network (KNN) b-tagger [14]. The KNN is designed to separate b-jets from c and light flavor jets.

C. Matrix Element Probabilities

In addition to kinematic distributions, we also consider matrix element probabilities (ME) as potential inputs to our final 2D-NNs. Matrix element discriminants were first employed in the search for $ZH \to \ell^+\ell^- b\bar{b}$ in [6], and are applied here with the same method of calculation. We compute matrix element probabilities for the processes $Z + jets$, $t\bar{t}$, and our signal.

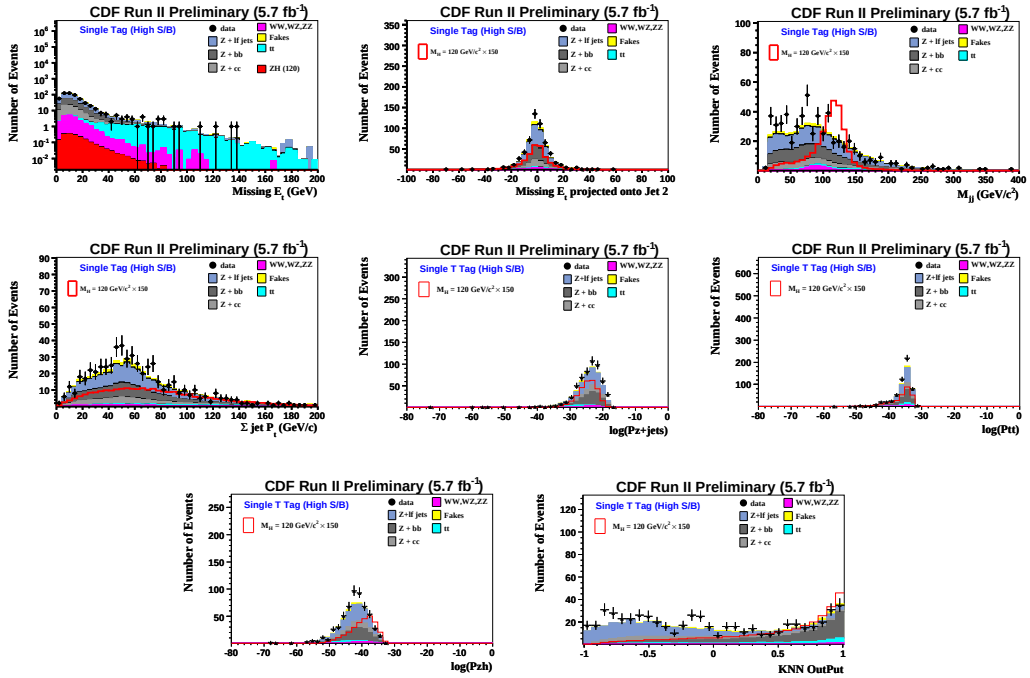

FIG. 4. NN input distributions for the single tight tag (T) category with high S/B selection.

D. Two-Dimensional NNs for S/B Discrimination

The two largest background classes at tag level are $Z + jets$-like events ($Z + b\bar{b}$, fakes, $Z + c\bar{c}$, mistagged b-jet events), and $t\bar{t}$. We train two dimensional JetNet [15] NNs to simultaneously separate signal events from $Z + jets$ and $t\bar{t}$. The NNs are designed to return two values (NNx, NNy) for a given event. For signal, the NN targets the values NNx=1, and NNy=0. For Z+jets, the NN targets NNx=0, and NNy=0. For $t\bar{t}$, the NN targets NNx=1, and NNy=1. We optimize three NNs (one for each tag category; see Table IV) with each NN trained on the same sample of signal (M_H = 120 GeV/c^2) and $t\bar{t}$ while the $Z + jets$ training samples are constructed to reflect the amount of light flavor, $b\bar{b}$, and $c\bar{c}$ events in each tag category.

Single Tight SecVtx	Loose SecVtx + 5% JetProb	Double Tight SecVtx
P_{jj}	$\not\!\!E_T$	$\not\!\!E_T$
$\not\!\!E_T$	M_{jj}	M_{jj}
P_{zh}	P_{tt}	P_{tt}
P_{tt}	P_{jj}	P_{zh}
M_{jj}	P_T(jet 1) + P_T(jet 2)	P_T(jet 1) + P_T(jet 2)
Karlsruhe Output		N jets
$\not\!\!E_T$ projection on Jet 2		Sphericity
P_T(jet 1) + P_T(jet 2)		

TABLE IV. The variables chosen by each neural network.

New to this iteration of the analysis is a change in this final two-dimensional discriminant binning. Previously, equal-sized bins of 20×20 were used. Now, a variable width 24×4 arrangement is used for greater sensitivity in the signal region and non-empty bins in the sparse region away from both signal and background (see Figure 10).

We utilize a sequential input algorithm which automatically selects the most powerful discriminants as NN inputs. This algorithm begins by forming single input NNs (considering all $\sim$ available inputs) and finds the single input which produces the best performing (lowest testing error) NN. Once the best single input is found, the algorithm loops through the remaining pool of inputs to find the best two input NN. The algorithm continues in this way until the addition of inputs not longer improves the testing error. Once the algorithm has found the optimal inputs for each b-tag category the final NNs are trained. The NN inputs can be seen in Figures 4 through 9.

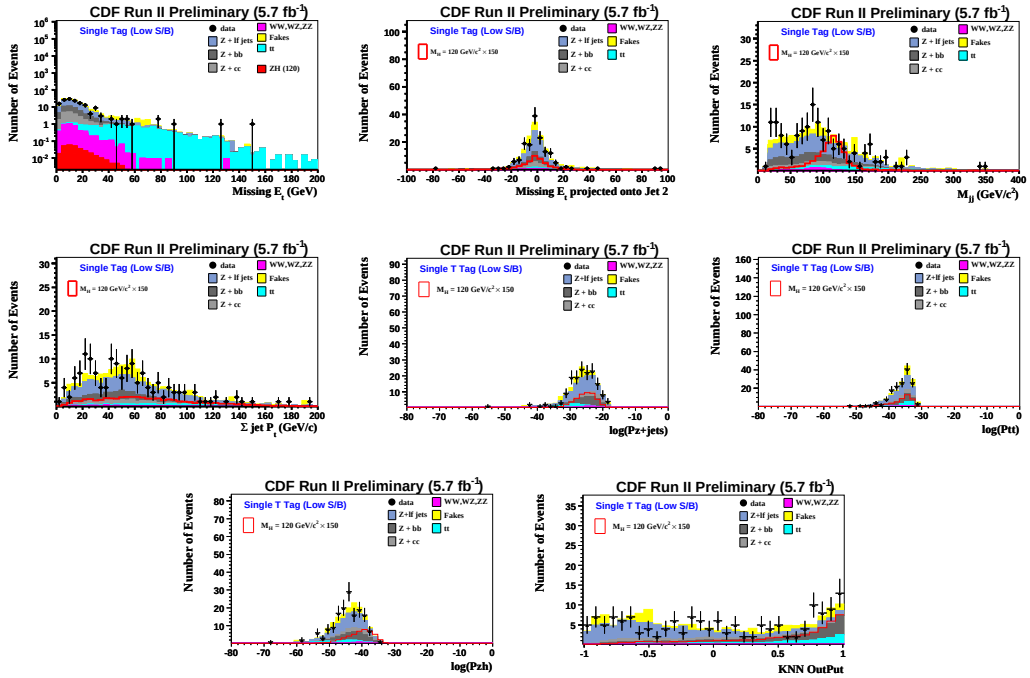

FIG. 5. NN input distributions for the single tight tag (T) category with low S/B selection.

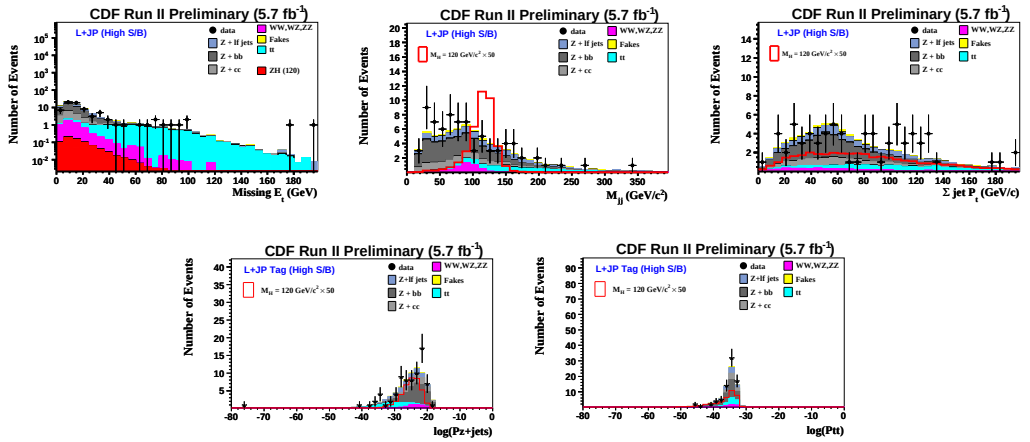

FIG. 6. NN input distributions for the loose plus JetProbability tag (L+JP) category with high S/B selection.

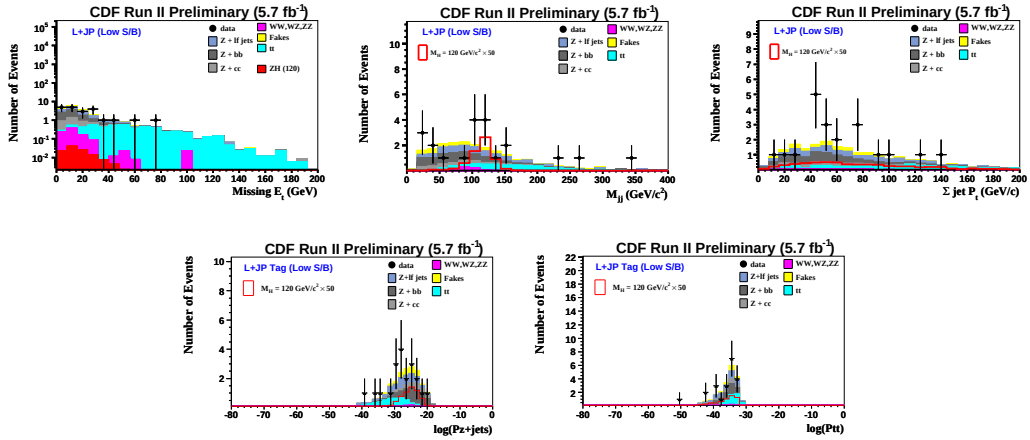

FIG. 7. NN input distributions for the loose plus JetProbability tag (L+JP) category with low S/B selection.

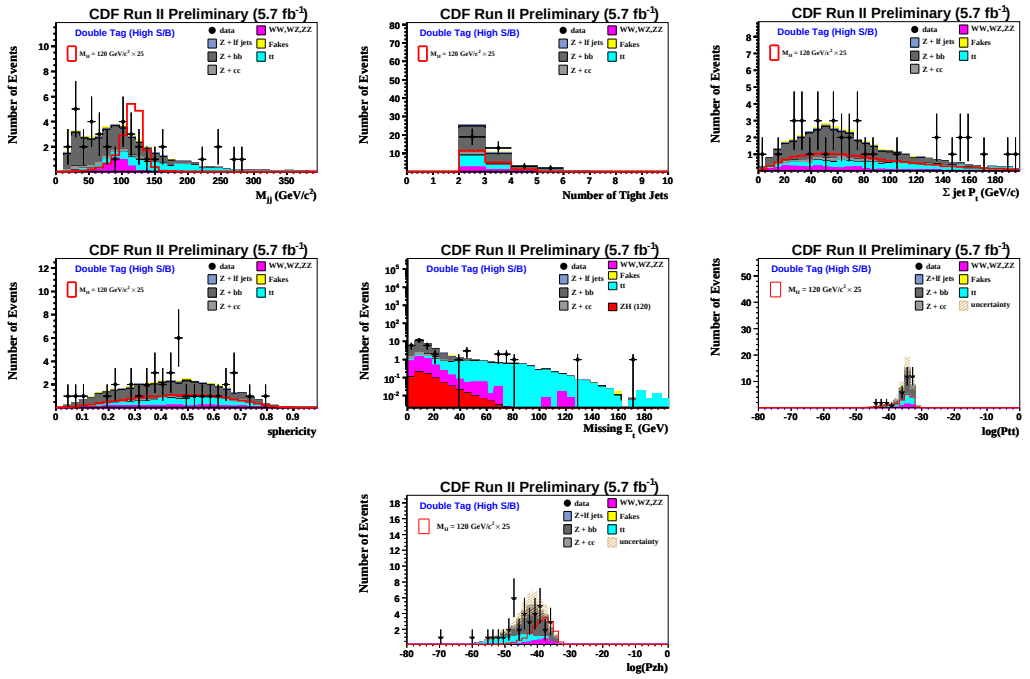

FIG. 8. NN input distributions for the double tight secondary vertex tag (TT) category with high S/B selection.

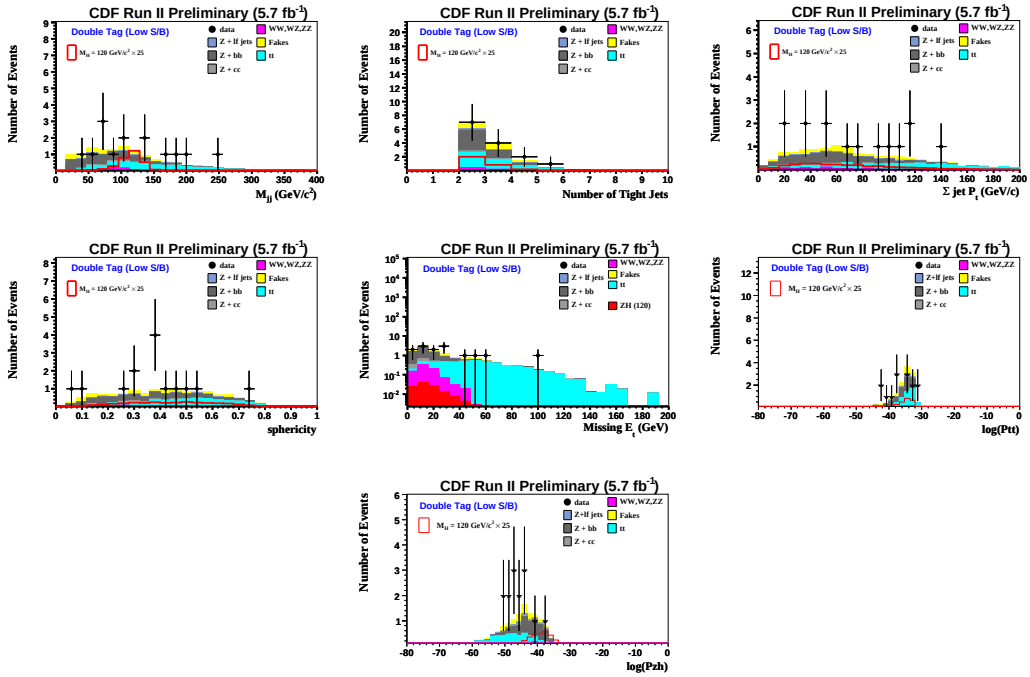

FIG. 9. NN input distributions for the double tight secondary vertex tag (TT) category with low S/B selection.

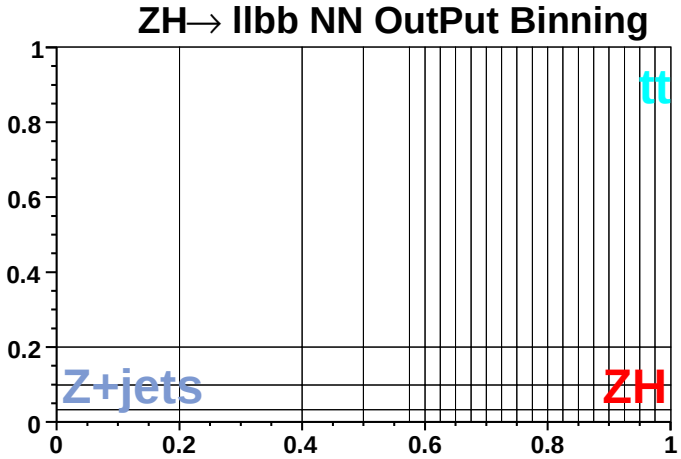

FIG. 10. The binning of the two-dimensional final analysis discriminant.

Systematic Uncertainty		Affected Samples
Tevatron $\mathcal{L}$	0.05	All MC
CDF $\mathcal{L}$	0.04	All MC
Z+h.f. σ	0.40	$Z + b\bar{b}$, $Z + c\bar{c}$
$t\bar{t}$ σ	0.10	$t\bar{t}$
Diboson σ's	0.06	ZZ, ZW, WW
Mistag errors	Hist. Shape & Acc	Mistags
Lepton ID	0.01	All MC
	0.04	All single tag MC
B-Tag scale factor	0.08	All double SecVtx tag MC
	0.11	All Loose + JP tag MC
Fakes	0.50	Fake ee, $\mu\mu$
JES	Hist. Shape & Acc	All MC
ISR & FSR	Hist. Shape & Acc	Signal MC
ZH σ	0.05	ZH MC
EM energy scale	0.015	All MC

TABLE V. Systematics currently applied in the analysis.

V. SYSTEMATICS

We assume a ∼5% uncertainty on the integrated luminosity and we aplly uncertainties of 4(T), 8(TT), and 11(L+JP)% to our b-tagged MC samples to account for the systematic errors associated with the calculation of b-tag efficiencies and scale factors. We apply 1% and 1.5% uncertainties on the trigger efficiency/lepton reconstruction and measured lepton energies. In order to cover the spread of fake rates measured from different jet-triggered data samples, we assign a 50% uncertainty on our total fake estimate. We apply a 40% uncertainty to $Z + b\bar{b}$ and $Z + c\bar{c}$ samples to cover the theoretical uncertainty on the Z + heavy flavor jets cross-section. Similarly, we apply a 6% cross-section uncertainty to all diboson samples, and 5% to signal. For $t\bar{t}$, we place a 10% uncertainty to account for both the theoretical uncertainty on the process cross-section and the difference between our simulated top mass (175 GeV/c^2) and current experimental measurements. We also consider uncertainties which are expected to affect both sample normalizations and the shape of the NN output distributions, such as the jet-energy scale (JES), the mount of initial/final state radiation (ISR/FSR), and the mistag event weights. Table V summarizes the systematic uncertainties applied in our limit calculations.

VI. RESULTS

After applying b-tagging, our final event totals are shown in Tables VI-VIII. The projected neural net output distributions for the signal regions are shown in Figures 11-14. We do not observe a significant excess over the number of events predicted by our background model, and proceed to quantify the maximum allowed ZH contamination in the data. We use the MCLIMIT [16] machinery for this, and do a binned fit of the 2D neural net distribution, including systematics. We set 95% confidence level upper limits on $\sigma_{ZH} \times BR(H \to b\bar{b})$ and compute observed limits for Higgs masses between 100 and 150 GeV/c^2 in 5 GeV intervals. The results are shown in Table IX, and Figure 15.

	High $S/\sqrt{B}$	Low $S/\sqrt{B}$
ZH	1.9 ± 0.2	0.3 ± 0.03
$t\bar{t}$	25.2 ± 3.3	13.8 ± 1.8
WW	0.2 ± 0.03	0.2 ± 0.02
WZ	6.3 ± 0.7	1.7 ± 0.2
ZZ	14.7 ± 1.6	2.7 ± 0.3
$Z \to \ell\ell + b\bar{b}$	146.8 ± 60.1	30.0 ± 12.3
$Z \to \ell\ell + c\bar{c}$	75.0 ± 30.7	15.7 ± 6.4
$Z \to \ell\ell + l.f.$	211.2 ± 27.5	66.6 ± 8.7
fakes	26.5 ± 13.2	32.4 ± 16.2
Total Bkg	505.9 ± 74.1	163.1 ± 23.1
Total Data	567	156

TABLE VI. Single tight SecVtx event totals.

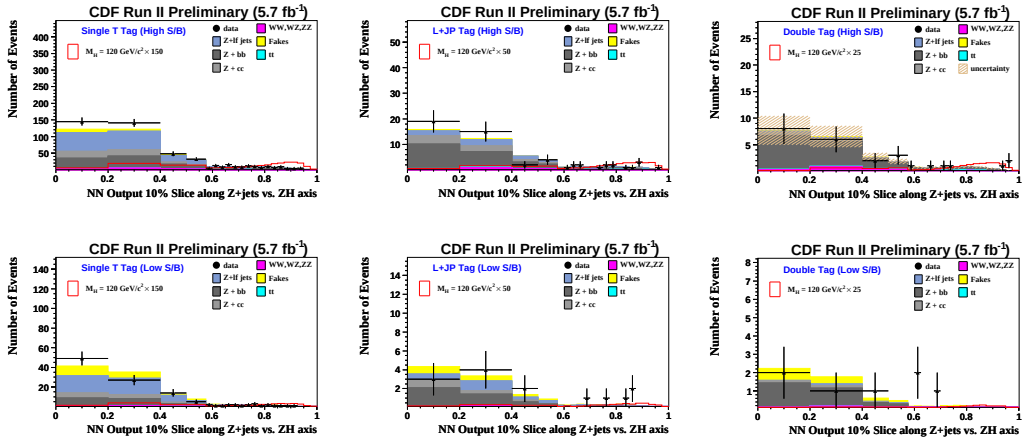

FIG. 11. NN output distributions for b-tagged events. These are projections of two dimensional NN outputs with a cut made (NNy<0.1) to highlight the most signal-like region.

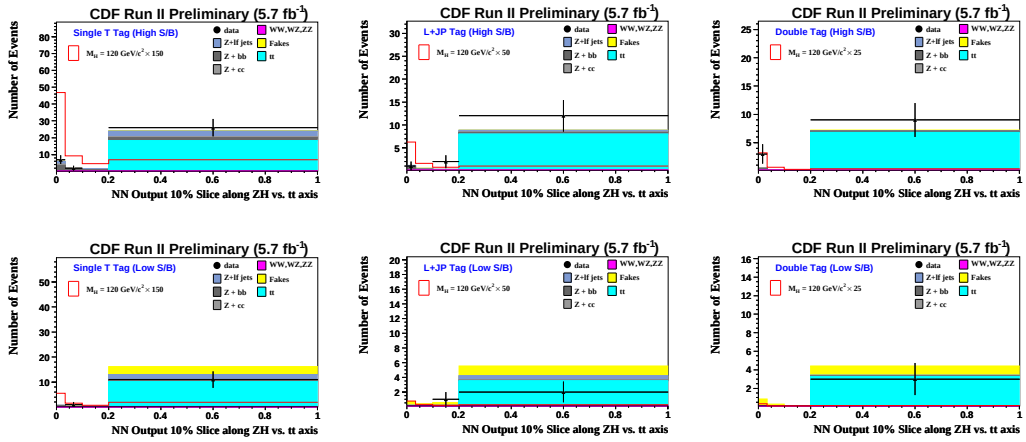

FIG. 12. Above are NN output projections on the ZH-$t\bar{t}$ axis with a cut made of NNx>0.9.

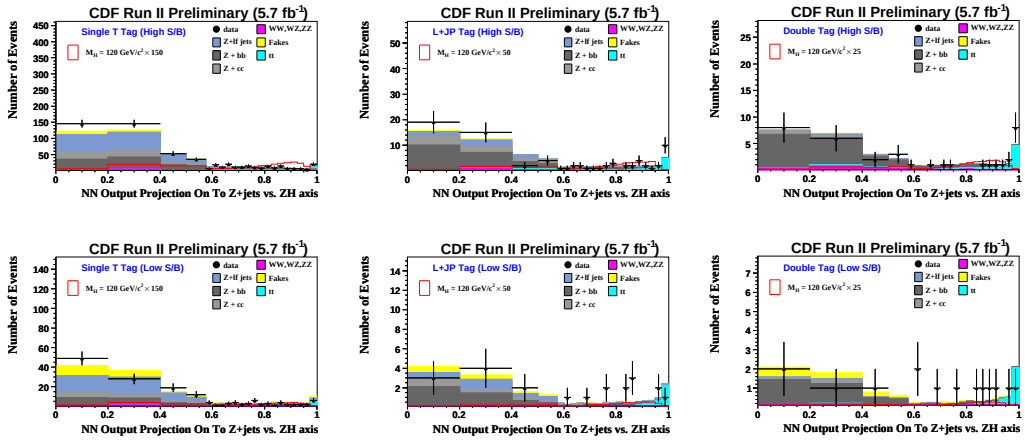

FIG. 13. Above are NN output projections of the complete outputs on the $Z + jets$-ZH axes.

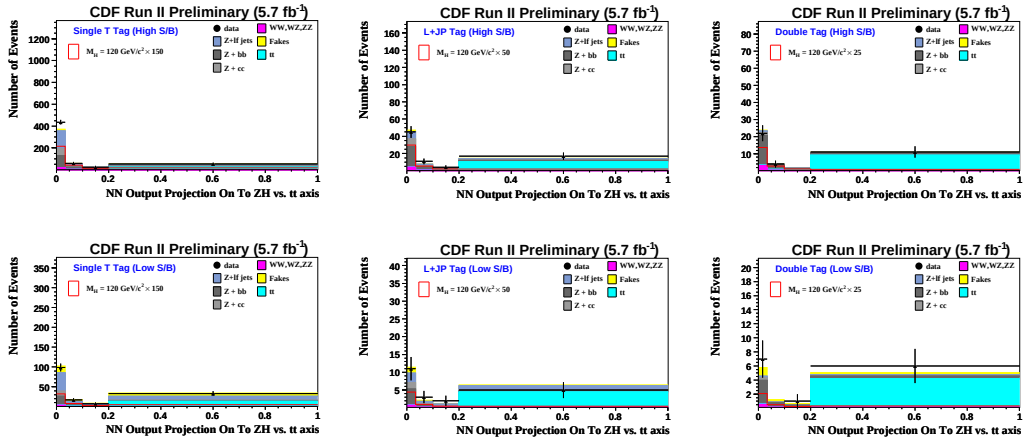

FIG. 14. Above are NN output projections of the complete outputs on the ZH-$t\bar{t}$ axes.

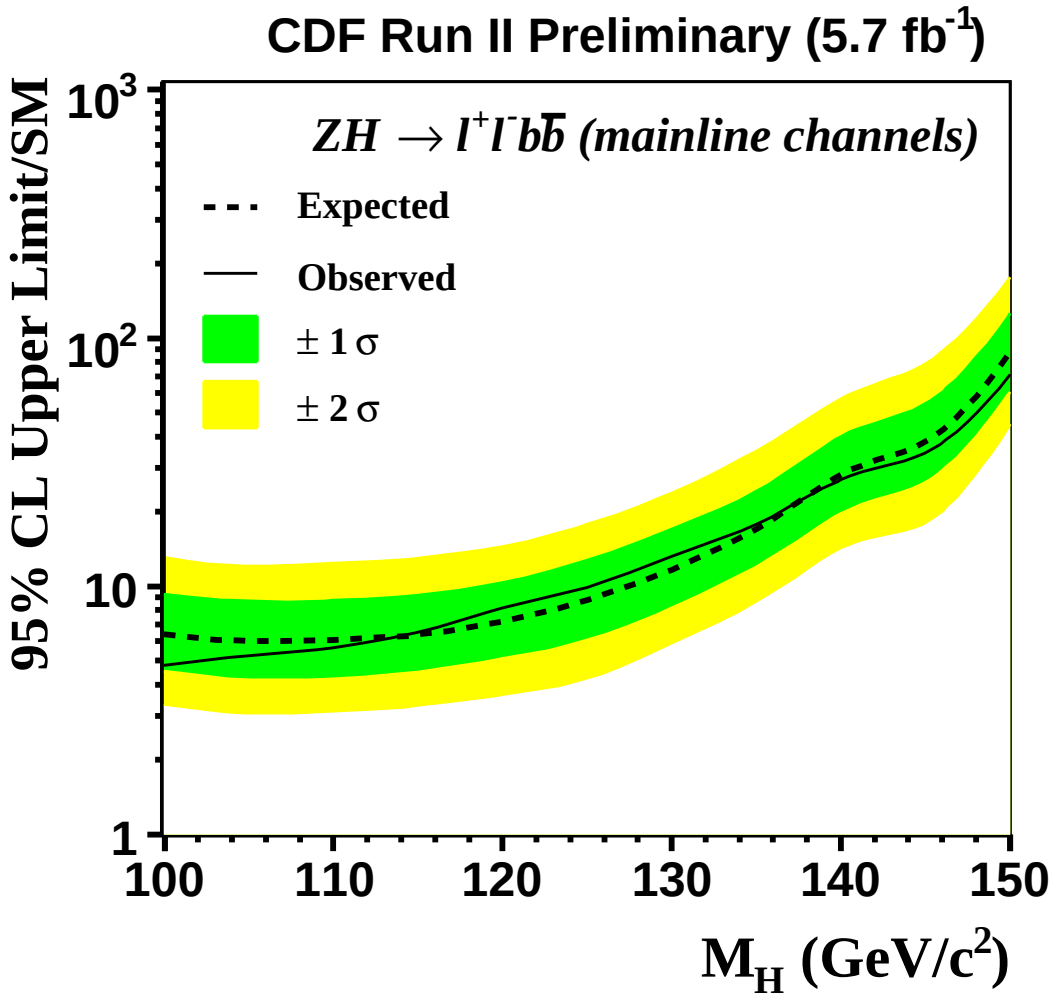

FIG. 15. Limits at the 95% confidence level.

	High $S/\sqrt{B}$	Low $S/\sqrt{B}$
ZH	0.8 ± 0.1	0.1 ± 0.02
$t\bar{t}$	11.6 ± 2.0	4.8 ± 0.8
WW	0.04 ± 0.01	0.02 ± 0.003
WZ	0.6 ± 0.1	0.1 ± 0.02
ZZ	4.4 ± 0.6	0.7 ± 0.1
$Z \to \ell\ell + b\bar{b}$	29.7 ± 12.5	5.7 ± 2.4
$Z \to \ell\ell + c\bar{c}$	11.0 ± 4.7	2.2 ± 0.9
$Z \to \ell\ell + l.f.$	13.0 ± 1.7	5.1 ± 0.7
fakes	2.5 ± 1.2	2.5 ± 1.3
Total Bkg	72.9 ± 13.7	21.2 ± 3.1
Total Data	77	21

TABLE VII. L + JP event totals.

	High $S/\sqrt{B}$	Low $S/\sqrt{B}$
ZH	0.7 ± 0.1	0.1 ± 0.02
$t\bar{t}$	9.9 ± 1.5	4.4 ± 0.7
WW	0.02 ± 0.003	0 ± 0.0
WZ	0.1 ± 0.02	0.03 ± 0.004
ZZ	3.6 ± 0.5	0.7 ± 0.1
$Z \to \ell\ell + b\bar{b}$	22.1 ± 9.2	4.6 ± 1.9
$Z \to \ell\ell + c\bar{c}$	2.4 ± 1.0	0.5 ± 0.2
$Z \to \ell\ell + l.f.$	1.2 ± 0.2	0.5 ± 0.1
fakes	0.9 ± 0.5	2.1 ± 1.0
Total Bkg	40.3 ± 9.4	12.7 ± 2.3
Total Data	37	14

TABLE VIII. Two Tight SecVtx event totals.

Mass (GeV/c^2)	Expected $^{+1\sigma(2\sigma)}_{-1\sigma(2\sigma)}$	Observed
100	5.68 $^{+2.71(6.64)}_{-1.69(3.01)}$	4.81
105	5.53 $^{+2.68(5.90)}_{-1.63(2.78)}$	5.15
110	5.65 $^{+2.55(6.25)}_{-1.68(2.83)}$	5.66
115	5.99 $^{+2.64(6.28)}_{-1.76(2.95)}$	6.54
120	6.97 $^{+3.07(7.15)}_{-2.11(3.46)}$	8.15
125	8.80 $^{+3.83(8.88)}_{-2.75(4.55)}$	9.88
130	11.65 $^{+5.37(12.05)}_{-3.47(5.73)}$	13.19
135	16.96 $^{+7.05(18.07)}_{-4.99(8.30)}$	17.75
140	26.37 $^{+11.50(27.16)}_{-8.24(13.51)}$	26.89
145	43.97 $^{+18.37(46.80)}_{-13.73(23.12)}$	38.91
150	87.43 $^{+38.00(87.91)}_{-26.81(42.26)}$	71.05

TABLE IX. Final discriminant limits at the 95% confidence level. The observed limits are run with 100,000 samplings while the expected limits are from 2500 pseudo-experiments with 1000 samplings.

VII. CONCLUSIONS

We have evaluated a new limit with an updated dataset 39% larger than in the previous analysis. We have calculated a 95% confidence level upper limits from 5.41 to 63.45 times the Standard Model prediction for Higgs Boson masses between 100 GeV/c^2 to 150 GeV/c^2. For a Standard Model Higgs boson mass of 120 GeV, we find the expected 95% confidence level upper limit to be 6.91 times the Standard Model prediction with an observed limit of 8.32.

ACKNOWLEDGMENTS

We thank the Fermilab staff and the technical staffs of the participating institutions for their vital contributions. This work was supported by the U.S. Department of Energy and National Science Foundation; the Italian Istituto Nazionale di Fisica Nucleare; the Ministry of Education, Culture, Sports, Science and Technology of Japan; the Natural Sciences and Engineering Research Council of Canada; the National Science Council of the Republic of China; the Swiss National Science Foundation; the A.P. Sloan Foundation; the Bundesministerium fuer Bildung und Forschung, Germany; the Korean Science and Engineering Foundation and the Korean Research Foundation; the Particle Physics and Astronomy Research Council and the Royal Society, UK; the Russian Foundation for Basic Research; the Comision Interministerial de Ciencia y Tecnologia, Spain; and in part by the European Community's Human Potential Programme under contract HPRN-CT-20002, Probe for New Physics.

---

[1] Higgs, P. "Broken Symmetries and the Masses of Gauge Bosons." Phys. Rev. Lett.131964508.
[2] Guralnik, G. S., C. R. Hagen, and T. W. B. Kibble. "Global Conservation Laws and Massless Particles." Phys. Rev. Lett.131964585.
[3] Englert, F. and R. Brout. "Broken Symmetry and the Mass of Gauge Vector Mesons." Phys. Rev. Lett.131964321.
[4] Strange, A., W. Marciano, and S. Willenbrock. "Higgs bosons at the Fermilab Tevatron." Phys. Rev. D4919941354.
[5] Hughes, R., *et. al. A Search for the Standard Model Higgs Boson in the Process* $ZH \to \ell^+\ell^- b\bar{b}$ *Using 4.1* fb^{-1} *of CDF II Data.* CDF Note 9889.
[6] Hughes, R., *et. al. A Search for* $ZH \to \ell^+\ell^- b\bar{b}$ *in 2.7*$^{-1}$ *using the Matrix-Element Method.* CDF Note 9718.
[7] We use a cylindrical coordinate system with z along the proton beam direction, r the perpendicular radius from the central axis of the detector, and ϕ the aximuthal angle. for θ, the polar angle from the proton beam, we define η = -ln tan ($\theta/2$). P_T refers to transverse momentum, while E_T denotes transverse energy.
[8] This trigger does not requie the calorimeter deposits be matched to an electron track.
[9] Harrington, R. D. "Measurement of the top quark mass in lepton+jets events with secondary vertex tagging." FERMILAB-THESIS-2007-25.
[10] Abulencia, A., *et. al.* "Measurement of the $t\bar{t}$ Production Cross Section in $p\bar{p}$ collisions at $\sqrt{s}$=1.96-TeV using Lepton + Jet Events with Jet Probability b-tagging." Phys. Rev. D742006072006.
[11] Mangano, M., *et. al.* "ALPGEN, a generator for hard multiparton processes in hadronic collisions." *J. High Energy Phys.* **07** (2003) 001.
[12] Sjöstrand, T., *et. al.* "High-Energy Physics Event Generation with PYTHIA 6.1." *Comput. Phys. Commun.* **135** (2001) 238.
[13] http://schwind.home.cern.ch/schwind/MLPfit.html
[14] Feindt, M., T. Muller, S. Richter, and Wolfgang Wagner. "A Neural Network b Tagger for Single-Top Analyses." CDF Note 7816.
[15] Peterson, C., T. Rognvaldsson, and L. Lonnblad. "JETNET 3.0: A Versatile artificial neural network package." *Comput. Phys. Commun.* **81** (1994) 185.
[16] Junk, T. "Confidence Level Computation for Combining Searches with Small Statistics." *Nucl. Instrum. Meth.* **A434** (1999) 435.